Supporting Information

Novel Perovskite-Based Betavoltaic Cell: Dual Additive Strategy for Enhanced $FAPbI_3$ α-phase Stability and Performance

Chol Hyun Kim†, Muhammad Bilal Naseem†, Junho Lee†, Hong Soo Kim, Sanghun Lee and Su-Il In*

Department of Energy Science & Engineering, Daegu Gyeongbuk Institute of Science & Technology (DGIST), 333 Techno Jungang-daero, Hyeonpung-eup, Dalseong-Gun, Daegu, 42988, Republic of Korea.

* Correspondence: S.-I. In (E-mail: insuil@dgist.ac.kr)

1. Experimental Section

1.1. Chemicals & Materials

Aqueous colloidal tin (IV) oxide solution (SnO_2, 15% in H_2O), ammonium hydroxide (NH_4OH, 28.0 ~ 30.0% NH_3) were purchased from Alfa Aesar. Lead (II) iodide (PbI_2, 99.99%) was purchased from TCI. Formamidinium iodide (FAI, > 99.99%), methylammonium chloride (MACl, > 99.99%) were purchased from greatcell solar materials. 9'-spirobifluorene (Spiro-MeOTAD, 99.8%), bis(trifluoromethane) sulfonimide lithium salt (LiTFSI, 99.8%), acetonitrile (ACN, 99.999%), 4-tert-butylpyridine (tBP, 98%), cesium chloride (CsCl, 99.99%), N,N-dimethylformamide (DMF, 99.8%), dimethyl sulfoxide (DMSO, 99.9%), diethyl ether (99.7%), chlorobenzene (CB, anhydrous 99.8%), and ^{12}C-citric acid (≥ 99.5%) were purchased from Sigma-Aldrich. ^{14}C-citric acid (1,5-14C, 50-60 mCi mmol^{-1}, EtOH: D.I water = 1 : 9) was purchased from American Radiolabeled Chemicals Inc. Ethyl alcohol (Anhydrous, 99.9%) was purchased from Daejung Chemicals & Metals Co., LTD. Carbon paste was purchased from KLK. Carbon powder was purchased from Xiamen TOB New Energy Technology Co., Ltd. All chemicals are used directly without further purification.

1.2. Preparation of the α-phase $FAPbI_3$ perovskite films

The fluorine-doped tin oxide (FTO) glass substrates (TEC-7, 7Ω sq^{-1}) were cleaned with detergent, deionized water, ethanol, and isopropanol by sonication, 10 min each. The cleaned FTO substrate was further treated with ultraviolet–ozone (UVO) for 30 min. A SnO_2 thin layer was deposited on the FTO substrate by spin coating the SnO_2 precursor solution (the stock solution was diluted with deionized water ratio 1:4 v/v%) at 4000 rpm for 30 s, which was annealed at 185 °C for 30 min at ambient atmosphere. The 1M solution was prepared by

dissolving 706 mg of the synthesized $FAPbI_3$ single crystal in 595.5 uL of N,N-dimethylformamide (DMF, 99.8%) and 79.4 uL of Dimethyl sulfoxide (DMSO 99.9%). For additive engineering, MACl, and dual additive of MACl and CsCl were added in the perovskite precursor, where 20 mol% (14.4mg) of MACl was added for the single additive device. For dual additive, 20 mol% (14.4 mg) of MACl and 10 mol% (9 mg) of CsCl for (MACl):(CsCl) = 4:1 was added in the perovskite precursor solution. The precursor solutions were stirred overnight at room temperature which was filtered by PTFE filter (0.2 μm pore size) before use. The SnO_2-coated FTO substrate was once again treated with UVO for 30 min prior to the deposition of perovskite precursor. The 50 μL of perovskite precursor solution was spread on the SnO_2-coated FTO substrate and rotate at first 1000 rpm for 10 sec and second 4000 rpm for 20 s. While spinning, 1 mL of diethyl ether was dripped on the rotating substrate 5 s before spin coating has finished. The films were annealed for 10 min at 150 °C, on which a spiro-MeOTAD (2,2′,7,7′-tetrakis(N,N-di-4-ethoxyphenylamino)-9,9′-spirobifluorene) layer was spin-coated at 4000 rpm for 30 s using the solution of 40.45 mg of spiro-MeOTAD, 19.5 μL of 4-tert-butylpyridine and 11.5 μL of lithium bis(trifluoromethylsulphonyl)imide (540 mg dissolved in 1 mL of acetonitrile) in 500 mL chlorobenzene. While spinning, 20μL of Spiro-MeOTAD solution was dripped on the rotating substrate 10 s after spin coating had started.

1.3. Preparation of the radioactive carbon nanoparticles/quantum dots (^{14}CNP/CQD)

The carbon nanoparticles and quantum dots were synthesized using a similar pyrolysis method as that in the previous report. The carbon layer was coated on the FTO glass substrate by a doctor-bladed technique. Afterwards, the electrode was sintered at 200 °C for 2 h on a hot plate, and then the impurities were blown out by nitrogen gas. To prepare the ^{14}CNP/CQD, 1 mL of ammonia solution was mixed with 10 mL of the ^{14}CA solution. Then 50

μL of precursor solution was poured dropwise on the carbon electrode with drying at 100 °C. After drying, the sample was sintered in a box furnace at 200 °C for 3 h, at a rate of 10 °C min^{-1}. The method for producing ^{12}CNP/CQD follows the same procedure as that used for ^{14}CNP/CQD, with the only difference being the substitution of the ^{12}CA solution for the ^{14}CA solution. the ^{12}CA solution comprised 4 mg ^{12}C-citric acid, 9 mL D.I. water, and 1 mL ethyl alcohol. The mixed solution has the same concentration as the radioactive isotope citric acid (^{14}C-citric acid, EtOH: D.I. water = 1: 9).

1.4. Assembly of a perovskite betavoltaic cell (PBC)

The carbon counter electrode was coated with carbon powder, and the perovskite working electrode was carefully pressed to match its dimensions. Subsequently, the electrodes were securely coupled by utilizing Teflon tape under tension.

1.5. Material Characterizations and Device Measurements

The surface, cross-sectional morphologies, and thickness of electrodes were analyzed at 3 kV and 10 μA using a field emission scanning electron microscope (FESEM, SU 8020, Hitachi). A transmission electron microscope (TEM, HF 3300, Hitachi,) was used to confirm the size and lattice spacing of the carbon quantum dots. The optoelectronic properties were measured by a UV-Visible spectrophotometer (UV-vis, Cary series, Agilent), photoluminescence (PL, FluoroMax Plus, Horiba). To obtain the phase and chemcial properties, a X-ray diffraction (XRD, Miniflex 600, Rigaku) was used along with a Panalytical, Empyrean X-ray diffractometer using Cu Kλ radiation (λ = 1.54 Å). Raman spectra of the carbon nanoparticles/quantum dots were obtained using a Raman spectrometer (Nicolet Almeca XR, Thermo Scientific) with a 532 nm laser for excitation. To confirm the performance of

photovoltaics and betavoltaics, a solar simulator (LCS-100, Oriel Sol), a potentiostat (Multi Autoalab, Metrohm), and a source meter (Keithley, 2635B, Keithley Instruments Inc.) was used. Based on the values obtained by source meter and potentiostat, the ECE and increase in the number of mobile electrons were calculated (**Equations S1-S3**).

Equation S1. Calculations for the energy conversion efficiency of betavoltaic cell.[1–3]

$$\eta = \frac{max}{\square_{\square\square\square}} \times 100\% = \frac{J_{sc} \times V_{oc} \times FF}{E_{avg} \times e \times A} \times 100\% \quad \textbf{(Eqn. 1)}$$

P_{max}: The maximum output power of the betavoltaic device (W)

P_{source}: The radiation power of the isotope carbon source (W)

FF: Fill factor

V_{oc}: Open-circuit voltage (V)

J_{sc}: Short-circuit current density (A cm^{-2})

A: Isotope carbon source per active surface area (mCi cm^{-2})

= 0.0045 mCi / 1.0 cm^2 = 0.0045 mCi cm^{-2}

1 Ci = 3.7 × 10^{10} Bq = 3.7 × 10^{10} Decay/s

E_{avg}: The average beta energy of the isotope (eV/Decay) = 49.4 keV/Decay for radioactive isotope of carbon

e: Electron charge (C)

Putting values in **Eqn. 1**

$$= \frac{15.010\ nA/cm^2 \times 2.750\ mV \times 0.584}{(49.4\ keV/Decay)(1.6 \times 10^{-19}\ C)(0.0045\ mCi/cm^2)} \times 100\%$$

$$= \frac{15.010\ nA \times 2.750\ mV \times 0.584\ \times (\frac{e}{1.6 \times 10^{-19}\ C}) \times (\frac{1.6 \times 10^{-19}\ C}{\square})}{(1.665 \times 10^5\ Decay/s) \times (7.904 \times 10^{-15}\ J/Decay)} \times 100\%$$

$$= \frac{(9.381 \times 10^{10}\ electron/s) \times (2.570 \times 10^{-22}\ J/electron)}{(1.665 \times 10^5\ electron/s) \times (7.904 \times 10^{-15}\ J/electron)} \times 100\%$$

$$= \frac{0.0241\ \square}{1.316\ \square\square} \times 100\% \cong 1.83\%$$

∴ Energy conversion efficiency of PBC: 1.83%.

Equation S2. Calculations for the increase in mobile electrons.[1]

$$\frac{\square\square\square\square\square\square\ \square\square\ \square\square\square\square\square\square\square\square\ \square\square\square\square\ \square\square\square\ \square\square\square}{\square\square\square\square\square\square} \quad \square\square\square\square\square\square\ \square\square\ \square\square\square\square\square\square\square\square\ \square\square\square\square\square\square\square\square\ \square\square\square\square\ \square\square\square\square\square\square\square\ \square\square\square\ \square\square\square\square\square\square\square = \frac{\square_{\square\square}}{\emptyset} \qquad \textbf{(Eqn. 2)}$$

I_{sc}: Short-circuit current (A)

∅: The isotope carbon source activity (mCi) = 0.0045 mCi

1 Ci = 3.7×10^{10} Bq = 3.7×10^{10} Decay/s

Putting values in **Eqn. 2**

$$= \frac{15.010\ \square\square}{(3.7\ \times 10^{7}\ Bq/mCi)(1\ Decay/Bq \cdot s)(0.0045\ mCi)}$$

$$= \frac{15.010\ nA \times (\frac{\square}{1.6 \times 10^{-19}\ C})}{(3.7\ \times 10^{7}\ Bq/mCi)(1\ Decay/Bq \cdot s)(0.0045\ mCi)(1\ electron/Decay)}$$

$$= \frac{9.381 \times 10^{10}\ electron/s}{1.665 \times 10^{5}\ electron/s}$$

$= 5.634 \times 10^{5} \cong 5.6 \times 10^{5}$

∴ Generated 5.6×10^{5} times more mobile electrons than generated by β-radiation only.

Equation S3. Calculations for energy generated from the radioactive isotope (^{14}C).[1]

Radioactive isotope carbon's average energy: 49.4 keV

P(0): Power emitted by the isotope at time (t = 0) from the radioactive source (W/Ci)

E(0): Energy emitted by the isotope at time (t = 0) from the radioactive source (J/s)

$(0) = \text{Average energy } (keV/Decay) \times 3.7 \times 10^{10}(Decay/s \cdot Ci) \times 1000\ (eV/keV) \times 1.6 \times 10^{-19}(J/eV)$

$= 292.448$ □□/□□

$(0) = P(0) \times 0.0045\ mCi = 1.316\ \times 10^{-9}\ J/s = 1.316\ nW$

∴ Energy generated from radioactive isotopes: 1.316 nW (using 0.0045 mCi).

This energy is 1.316 × 10^{-10} times lower than the light energy on the active surface area of 1.0 cm^2 (1000 W/m^2 × 1.00 cm^2 = 0.1 W).

2. Characterization

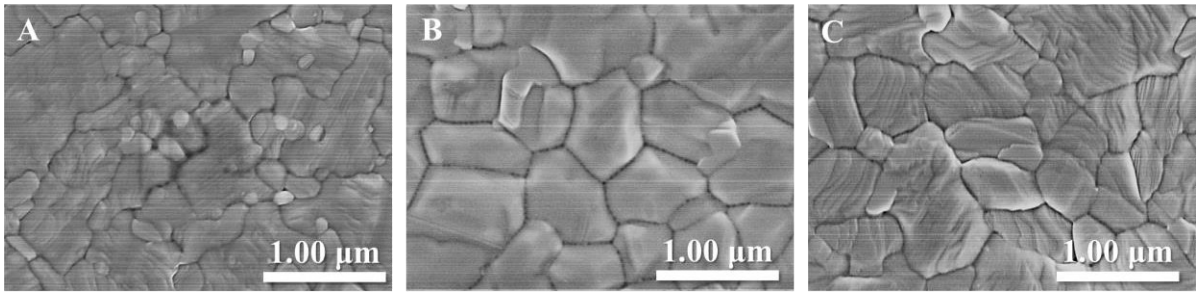

Figure S1. FESEM images of (A) $FAPbI_3$, (B) MACl-$FAPbI_3$, and (C) MACl/CsCl-$FAPbI_3$ films.

Compared to bare $FAPbI_3$, the films treated with MACl and MACl/CsCl additives showed a homogeneous and compact structure, with large grain sizes of approximately 700 and 750 nm, respectively. This improvement can be attributed to the presence of chloride (Cl^-) anions from the additives, which facilitate grain growth and promote a preferred orientation of the perovskite grains[4].

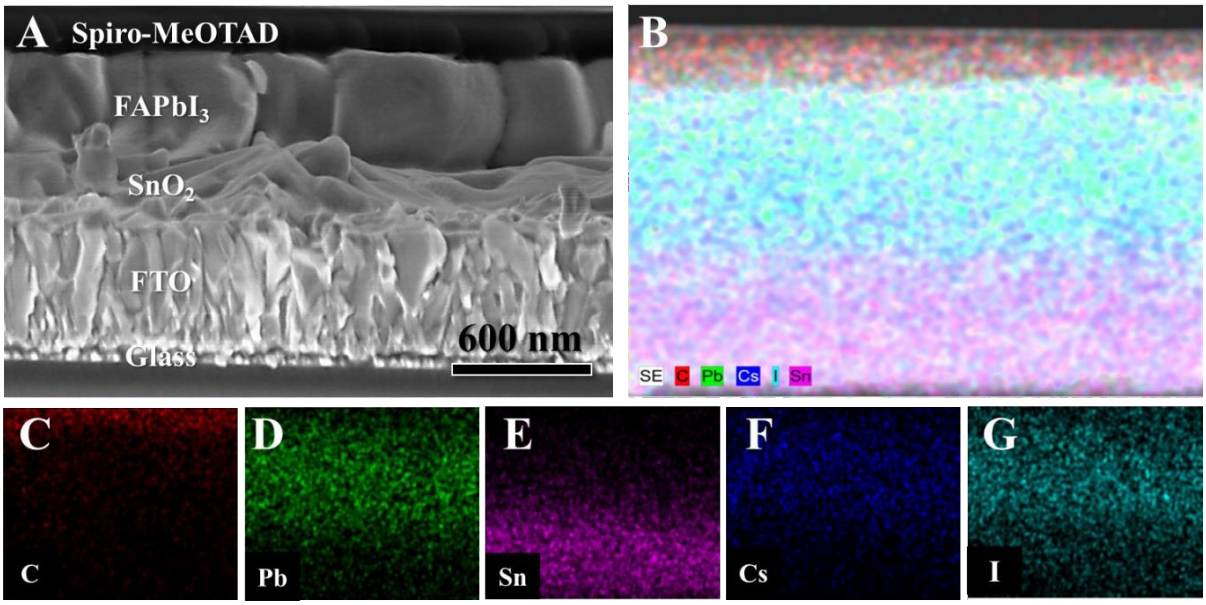

Figure S2. (A) FESEM image of the MACl/CsCl-$FAPbI_3$ cross-section side view. (B-G) EDS mapping images of the MACl/CsCl-$FAPbI_3$ film.

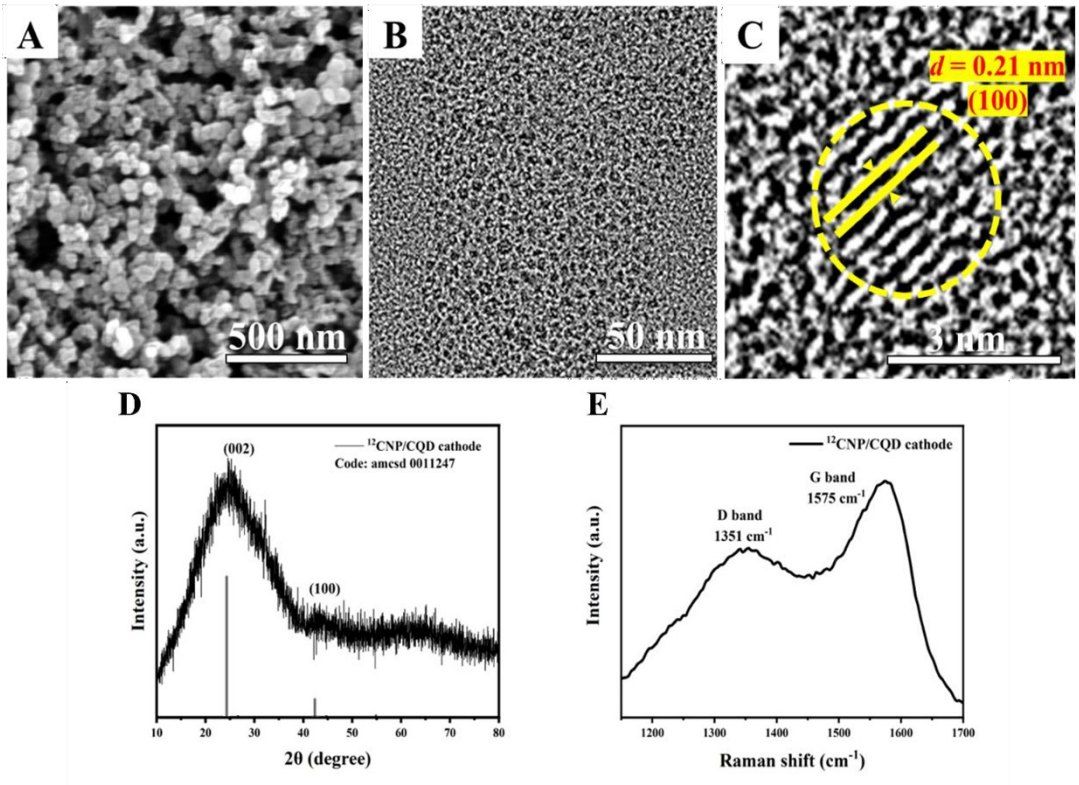

Figure S3. (A) FESEM, (B) and (C) TEM images of normal carbon nanoparticles/quantum dots (^{12}CNP/CQD). (D) XRD and (E) Raman spectroscopy of normal ^{12}CNP/CQD.

As shown in Figures S3A-C, the 12CNP/CQD particles are uniformly distributed, forming graphitic crystal structures in the (100) plane with an average diameter of 3.14 nm. These characteristics were further confirmed by XRD and Raman spectroscopy (Figures S3D and S3E). The XRD spectrum of 12CNP/CQD revealed two distinct peaks at 24.7° and 42.7°, corresponding to the (002) and (100) planes of hexagonal graphite, respectively[5,6]. Raman spectroscopy showed D- and G-band peaks at 1351 and 1575 cm^{-1}, respectively, with a D/G intensity ratio (ID/IG) of 0.70. These results confirm the successful fabrication of 14CNP/CQD as compared from our previous work[1]. This indicates low defect density and high material quality[7,8]. Collectively, these results suggest that the ^{12}CNP/CQD-based cathode exhibits a high surface area and porous structure, which could enhance β-radiation energy emission per unit area and improve electron transport efficiency.

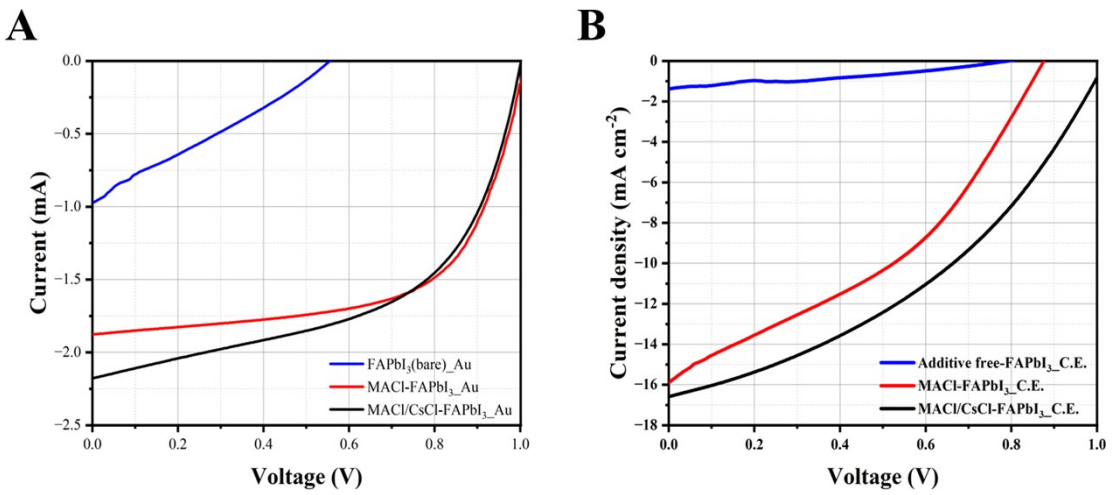

Figure S4. (A) *I-V and* (B) *J-V* performance of the $FAPbI_3$-based perovskite photovoltaics under AM 1.5 light irradiation.

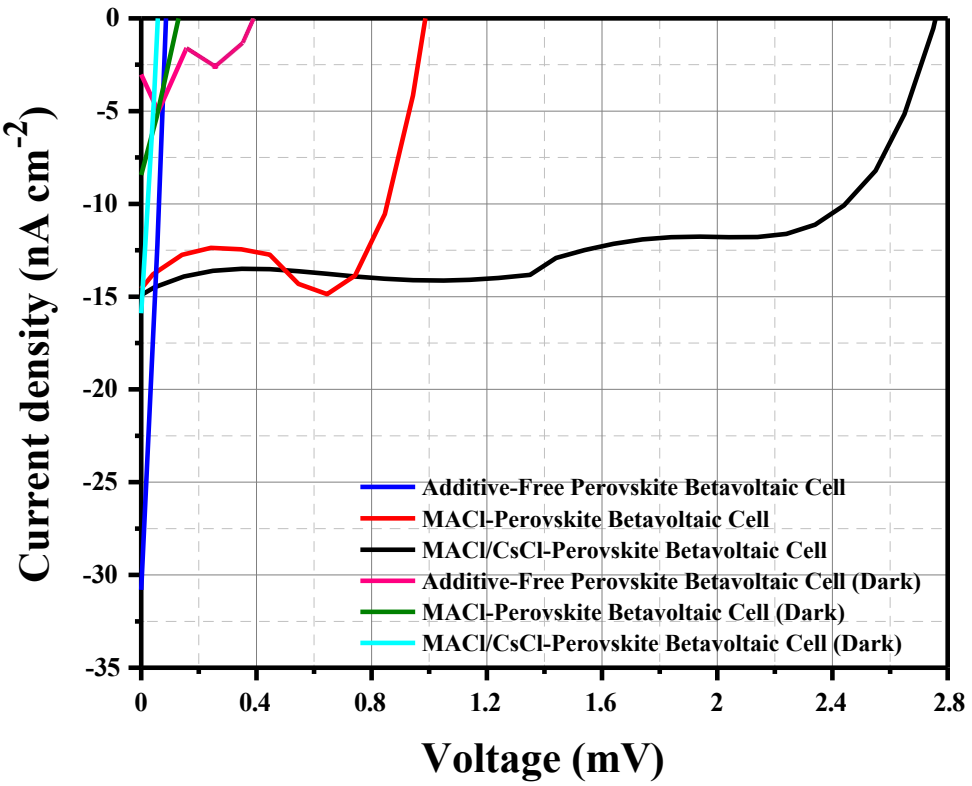

Figure S5. *J-V* curve and dark characteristics of $FAPbI_3$-based perovskite cells.

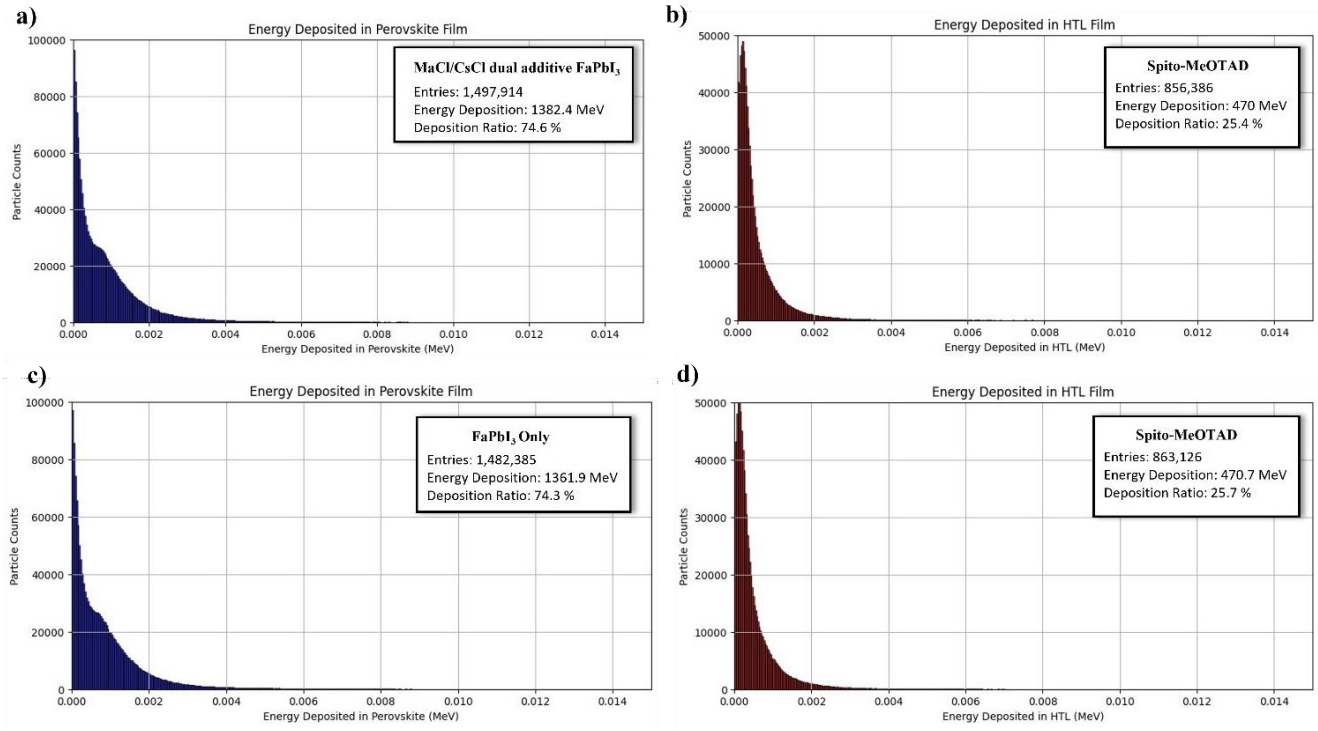

Figure S6. Energy deposition profiles of C-14 beta particles on different films of the dual-additive and $FAPbI_3$ only PBC, a) MACl/CsCl dual additive $FaPbI_3$ perovskite film, b) Spiro-MeOTAD HTL film, c) $FAPbI_3$ only Perovskite film, and d) Spiro-MeOTAD HTL film.

Table S1. International safety regulations of nuclear materials handling. Reproduced with permission from ref. 1, Copyright 2020, Royal Society of Chemistry.

<table>
<tr><th></th><th>Article</th></tr>
<tr><td>NUCLEAR SAFETY ACT</td><td>Article 2 (Definitions)
The terms used in this Act shall be defined as follows:<Amended by Act No. 11715, Mar.23, 2013; Act No. 12666, May 21, 2014; Act No. 13078, Jan. 20, 2015; Act No. 1338, Jun. 22, 2015; Act No. 13616, Dec. 22, 2015>
3. The term "nuclear fuel materials" means materials prescribed by Presidential Decree that produce nuclear energy, such as uranium and thorium;
4. The term "nuclear raw materials" means uranium ore, thorium ore, and other materials prescribed by Presidential Decree, used as raw materials for nuclear fuel materials;
6. The term "radioactive isotope" means an isotope which emits radiation and what is prescribed by Presidential Decree among any combination thereof;</td></tr>
<tr><td>ENFORCEMENT DECREE OF THE NUCLEAR SAFETY ACT</td><td>Article 5 (Radioisotopes)
"Isotope prescribed by Presidential Decree" in subparagraph 6 of Article 2 of the Act means any substance for which the quantity and concentration of an isotope exceed such quantity and concentration as determined by the Commission, excluding the following substances:
1. Nuclear fuel material referred to in subparagraph 3 of Article 2 of the Act;
2. Nuclear source material referred to in subparagraph 4 of Article 2 of the Act;
3. Radioactive material or apparatuses in which radioactive material is embedded, which poses no risk of radiation hazard as determined and publicly notified by the Commission.</td></tr>
<tr><td>STANDARD OF RADIATION PROTECTION</td><td>Article 9 (Quantity and Concentration of Radioisotopes)
"Quantity and concentration as prescribed by the Nuclear Safety and Security Commission" as provided for in Article 5 of the Decree shall be the quantity in column 3 and the concentration in column 4 for the relevant radionuclides in column 2 of Table 5.
<table>
<tr><th colspan="4">Quantity and Specific Activity of Radioisotopes for Exemption [Table 5]</th></tr>
<tr><th>Atomic number
[Column 1]</th><th>Isotopes
[Column 2]</th><th>Minimum Quantity, (Bq)
[Column 3]</th><th>Minimum Specific Activity
(Bq/g)
[Column 4]</th></tr>
<tr><td>6</td><td>C-14</td><td>1×10^7</td><td>1×10^4</td></tr>
</table></td></tr>
<tr><td>Regulations on Technical Standards for Radiation Safety Control, Etc.</td><td>Article 37 (Use and Distribution)
Technical standards as regards the use or distribution of unsealed sources shall be as follows:
1. Unsealed sources shall be used or distributed at use facilities or work rooms.</td></tr>
</table>

Table S2. Comparison of characteristic parameters from the perovskite photovoltaic cell concerning the control cell under AM 1.5 illumination (light).

Sample name	Energy source (mW m^{-2})	Open-circuit voltage V_{oc} (V)	Short-circuit current density J_{sc} (mA cm^{-2})	Maximum power density P_{max} (mW cm^{-2})	Fill Factor (%)	Total Efficiency η (%)
FTO/SnO_2/$FAPbI_3$/Spiro-MeOTAD/Au	1000	0.55	0.97	2.0	27	2.0
FTO/SnO_2/$FAPbI_3$/Spiro-MeOTAD/^{12}CNP/CQD/FTO	1000	0.79	1.37	0.4	35	0.4
FTO/SnO_2/MACl-$FAPbI_3$/Spiro-MeOTAD/Au	1000	0.91	1.88	15.8	69	15.8
FTO/SnO_2/ MACl-$FAPbI_3$/Spiro-MeOTAD/^{12}CNP/CQD/FTO	1000	0.88	15.85	5.3	38	5.3
FTO/SnO_2/ MACl/CsCl-$FAPbI_3$/Spiro-MeOTAD/Au	1000	1.01	2.18	15.9	54	15.9
FTO/SnO_2/ MACl/CsCl-$FAPbI_3$/Spiro-MeOTAD/^{12}CNP/CQD/FTO	1000	1.02	16.60	6.7	39	6.7

Table S3. Comparison of characteristic parameters from the perovskite betavoltaic cell (PBC) concerning the control cell.

Sample name	Radioactive source (mCi)	Open-circuit voltage V_{oc} (mV)	Short-circuit current density J_{sc} (nA cm^{-2})	Maximum power density P_{max} (nW cm^{-2})	Fill Factor (%)	Total Efficiency η (%)
FTO/SnO_2/$FAPbI_3$/Spiro-MeOTAD/^{14}CNP/CQD/FTO	^{14}C, 0.0045 (Cathode)	0.01	30.36	0.0001	30	0.07
FTO/SnO_2/MACl-$FAPbI_3$/Spiro-MeOTAD/^{14}CNP/CQD/FTO	^{14}C, 0.0045 (Cathode)	0.94	15.20	0.011	77	0.83
FTO/SnO_2/MACl/CsCl-$FAPbI_3$/Spiro-MeOTAD/^{14}CNP/CQD/FTO	^{14}C, 0.0045 (Cathode)	2.75	15.01	0.024	58	1.83

Table S4. Comparison with previous works reporting betavoltaic cells and their properties.

Structure of betavoltaic cell	Radioactive source (mCi)	Open-circuit voltage V_{oc} (mV)	Short-circuit current density J_{sc} (nA cm^{-2})	Maximum Power density P_{max} (nW cm^{-2})	Power density per radioactive source (nW cm^{-2} mCi^{-1})	Efficiency η (%)	Published year	Reference
$Al_{0.52}In0_{.48}P$ based PIN junction	^{63}Ni, 5 mCi	530	1.77	20.24	0.04	6.60	2016	[9]
4H-SiC based PN junction	^{63}Ni, 1 mCi	720	16.8	6.17	6.17	6.00	2016	[10]
Black TiO_2 nanotube arrays (TiO_2 NTAs) based Schottky junction	^{63}Ni, 20 mCi	1,130	103.3	37.0	1.85	3.65	2018	[11]
TiO_2 nanotube arrays (TNTAs) electrochemically reduced in ethylene glycol electrolyte (EGECR-TNTAs) based Schottky junction	^{63}Ni, 20 mCi	1,040	117.5	39.2	1.96	3.79	2018	[12]
Metallic single-walled carbon nanotubes (m-SWCNTs)/ZnO nanorod arrays (ZNRAs) based Schottky junction	^{63}Ni, 20 mCi	510	38.19	7.78	0.389	3.58	2020	[13]
Single-wall carbon nanotubes (SWCNTs)@Gray color-TiO_2 nanotube arrays (GTNRAs) with I^-/I_3^- electrolyte	^{63}Ni, 20 mCi	262.7	870	90.07	4.50	8.74	2022	[14]
ZrO_2@Ar-TiO_2 nanorod arrays (TNRAs) with I^-/I_3^- electrolyte	^{63}Ni, 10 mCi	276.0	1041	97.70	9.77	9.27	2022	[15]
MACl/CsCl-FAPbI$_3$ Perovskite betavoltaic cell (PBC)	***^{14}C, 0.0045 mCi***	***2.75***	***15.01***	***0.024***	***5.32***	***1.83***	***This work***	**-**

* The information is based on the manufactured betavoltaic cells.

References

1 Y. Hwang, Y. H. Park, H. S. Kim, D. H. Kim, S. Ali, S. Sorcar, M. C. Flores, M. R. Hoffmann and S.-I. In, *Chem. Commun.*, 2020, **56**, 7080–7083.

2 T. Wacharasindhu, J. W. Kwon, D. E. Meier and J. D. Robertson, *Appl. Phys. Lett.*, 2009, **95**, 1, 014103.

3 Z. Song, C. Zhao, F. Liao and Y. Zhao, *ACS Appl. Mater. Interfaces*, 2019, **11**, 32969–32977.

4 I. S. Yang and N. Park, *Adv. Funct. Mater.*, 2021, **31**, 2100396.

5 Z. Q. Li, C. J. Lu, Z. P. Xia, Y. Zhou and Z. Luo, *Carbon N. Y.*, 2007, **45**, 1686–1695.

6 H. Wang, C. Sun, X. Chen, Y. Zhang, V. L. Colvin, Q. Rice, J. Seo, S. Feng, S. Wang and W. Y. William, *Nanoscale*, 2017, **9**, 1909–1915.

7 Z. Wang, L. Cao, Y. Ding, R. Shi, X. Wang, H. Lu, Z. Liu, F. Xiu, J. Liu and W. Huang, *RSC Adv.*, 2017, **7**, 21969–21973.

8 A. Dager, A. Baliyan, S. Kurosu, T. Maekawa and M. Tachibana, *Sci. Rep.*, 2020, **10**, 12333.

9 S. Butera, G. Lioliou, A. B. Krysa and A. M. Barnett, *J. Appl. Phys.*, 2016, **120**, 144501.

10 C. Thomas, S. Portnoff and M. G. Spencer, *Appl. Phys. Lett.*, 2016, **108**, 013505.

11 N. Wang, Y. Ma, J. Chen, C. Chen, H. San, J. Chen and Z. Cheng, *Nanoscale*, 2018, **10**, 13028–13036.

12 Y. Ma, N. Wang, J. Chen, C. Chen, H. San, J. Chen and Z. Cheng, *ACS Appl. Mater. Interfaces*, 2018, **10**, 22174–22181.

13 C. Chen, J. Chen, Z. Wang, J. Zhang, H. San, S. Liu, C. Wu and W. Hofmann, *J. Mater.*

Sci. Technol., 2020, **54**, 48–57.

14 N. Wang, R. Zheng, T. Chi, T. Jiang, Z. Ding, X. Li, S. Liu, L. Zhang and H. San, *Compos. Part B Eng.*, 2022, **239**, 109952.

15 R. Zheng, Z. Ding, W. Wang, N. Wang, Z. Wang, T. Jiang, X. Li, S. Liu, L. Zhang and H. San, *Appl. Surf. Sci.*, 2023, **611**, 155757.

The main text and the supporting information (SI) have been proofread by a professional English editing service with native speakers.

Certificate of Editing

This Certifies That

Novel Perovskite-Based Betavoltaic Cell: Dual Additive Strategy for Enhanced FAPbI3 α-phase Stability and Performance

By Chol Hyun Kim, Muhammad Bilal Naseem, Junho Lee, Hong Soo Kim, Sanghun Lee and Su-Il In

was edited for grammar and clarity. The authors' original ideas were not edited in any way.

CY PLUS

www.cyplus.co.kr